Researches in Mathematics and Mechanics. 2026. Vol. 31, iss. 1(47). P. 81–97.

UDC 519.87:616-006

O. D. Rapchynskyi, *PhD Student*
Odesa Polytechnic National University
Department of Applied Mathematics and Information Technologies
1 Shevchenka Avenue, Odesa, 65044, Ukraine
e-mail: 6258036@as.op.edu.ua
ORCID iD: https://orcid.org/0009-0003-3702-7370
O. D. Kichmarenko, *Doctor of Physical and Mathematical Sciences, Professor*
Military Academy (Odesa)
Department of Fundamental Sciences
10 Fontanska Doroha, Odesa, 65009, Ukraine
e-mail: olga.kichmarenko@gmail.com
ORCID iD: https://orcid.org/0000-0002-7388-4922
A. O. Stekhun, *Candidate of Physical and Mathematical Sciences, Associate Professor*
Odesa I. I. Mechnikov National University
Department of Optimal Control and Economic Cybernetics
2 Zmiienka Vsevoloda St, Odesa, 65082, Ukraine
e-mail: a.stehun@onu.edu.ua; angela.stehun@gmail.com
ORCID iD: https://orcid.org/0000-0003-3140-2689

DISCRETE CELLULAR AUTOMATA MODELS OF TUMOR GROWTH DYNAMICS AND IMMUNE SURVEILLANCE

Mathematical modeling and simulation play a central role in elucidating tumor growth dynamics and evaluating therapeutic interventions in oncology. A cellular automata approach consisting of three discrete models of increasing complexity was investigated: (i) an uncontrolled proliferation model capturing exponential tumor expansion; (ii) a spatially constrained proliferation model reproducing logistic-like saturation due to microenvironmental limits; and (iii) an immune response model incorporating effector cell interactions and cytokine-mediated chemotaxis. These models operate on two-dimensional lattices with stochastic update rules calibrated by biologically relevant division and death rates. Simulation experiments demonstrate that the uncontrolled model reproduces classical exponential growth behavior, while the spatially constrained model yields sigmoidal growth curves consistent with Verhulst dynamics. The immune response model further enables simulation of

interactions among tumor cells, effector lymphocytes, and cytokine signals, capturing complex biological dynamics that are difficult to derive or compute with traditional analytical methods. Parameter sensitivity analyses reveal critical regimes of cytokine secretion and effector recruitment that govern the transition between tumor containment and escape. This discrete, rule-based model provides a powerful tool for exploring tumor-immune interactions and evaluating potential treatment strategies.

MSC: 92C50, 92C37, 68Q80.

Keywords: cellular automata, tumor growth, simulation, immune response, chemotaxis.

DOI: https://doi.org/10.18524/2519-206X.2026.1(47).364555

Received: 15.03.2026. *Accepted for publication:* 27.03.2026.

Published: 15.09.2026.

Introduction

Mathematical and computer models are vital tools in cancer research. They can show how tumors grow, spread, and respond to treatments in ways that are difficult to capture with traditional equations. Cellular automata (CA) are simple grid models where each cell follows a few basic rules [1; 2]. Even with these simple rules, CA can display complex patterns because cells interact with each other and their environment.

Analytical models face difficulty in incorporating the full spectrum of complex cell-cell and cell-environment interactions, and their complexity grows rapidly as new biological details are added. In many practical applications, sufficiently accurate simulations can provide reliable insight without requiring closed-form solutions. CA simulations overcome these challenges by tracking each cell on a lattice, updating its state based on probabilistic rules for division, death, movement, and immune interaction. Computer simulations enable systematic exploration of parameter spaces and sensitivity analyses to identify threshold effects and critical transitions.

This work examines three CA models with growing complexity: uncontrolled growth, space-limited growth, and immune-driven tumor suppression. Our simulations show that simple rules can produce familiar growth curves: exponential growth in the first model and S-shaped (logistic [3]) growth in the second. The third model illustrates how immune cell lifespan, chemical signals,

and arrival rate affect tumor control [4; 5]. The goals are to demonstrate the usefulness of CA in cancer modeling and confirm known growth laws.

Main Results1. Model of uncontrolled cancer cell proliferation

Let $x_{i,j}(t) \in \{0,1\}$ denote the presence of a tumor cell at lattice site (i,j) at discrete time t. The lattice is unbounded, and time advances in uniform steps of length Δt, where T_d is the mean time between cell divisions.

Cell division follows a Poisson (memoryless) process with rate $1/T_d$, giving the probability of a division event in one time step as

$$p_d = 1 - e^{-\frac{\Delta t}{T_d}}. \tag{1}$$

This form comes from the fact that the expected number of division events in interval Δt is $\Delta t/T_d$, and the exponential distribution yields $1-e^{-\Delta t/T_d}$ as the chance of at least one event.

Initially, a single cancer cell occupies the origin:

$$x_{0,0}(0) = 1, \quad x_{i,j}(0) = 0 \quad (i,j) \neq (0,0). \tag{2}$$

At each time step, each occupied site divides with probability p_d, placing a daughter cell on a randomly chosen empty von Neumann neighbor. We then define the total tumor size by

$$X(t) = \sum_{i,j} x_{i,j}(t), \tag{3}$$

which under these rules exhibits exponential growth on average. This behavior corresponds to classical exponential tumor growth models [1; 6–8].

Simulation of uncontrolled tumor growth.

Tumor expansion without spatial constraints or competition was simulated on an unbounded lattice up to $t = 500$ days with $\Delta t = 1$ day and $T_d = 5$ days. Snapshots at $t = 125, 250, 375, 500$ days are shown in Fig. 1. For mean division times $T_d \in \{5,6,7,8\}$ days ($\Delta t = 1$ day), the tumor size $X(t)$ was computed up to $t = 1000$ days (Fig. 2), and the values appear in Table 3.

2. Model of spatially constrained proliferation

In many solid tumors the available space for cell growth is limited by the surrounding tissue [9; 10]. To account for spatial constraints, we restrict the

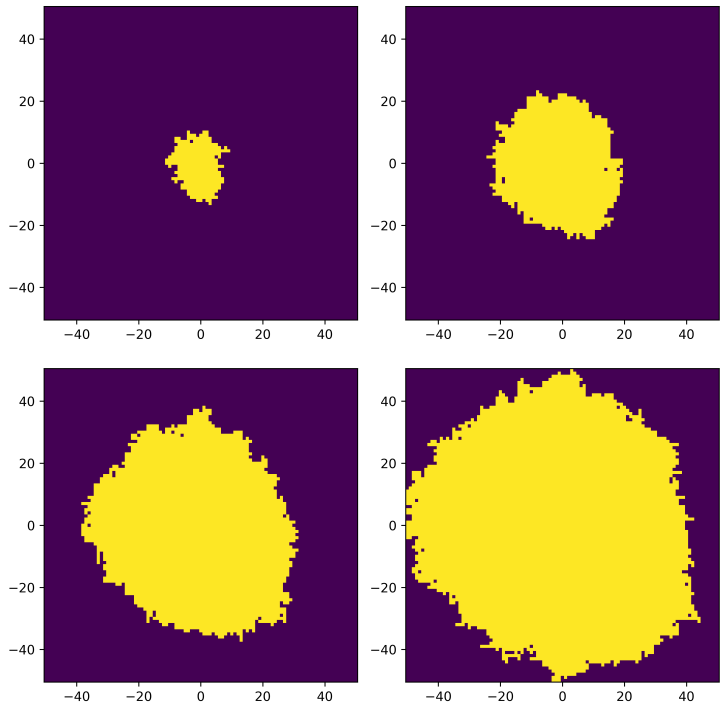

Figure 1: Snapshots of cell distribution at $t = 125, 250, 375, 500$ days under uncontrolled growth on an unbounded lattice.

Table 3: Tumor size $X(t)$ at various time points for different mean division times T_d.

T_d (days)	$t = 250$	$t = 500$	$t = 750$	$t = 1000$
5	1437	6533	16021	29534
6	1044	4909	11665	21430
7	612	3231	8184	15169
8	590	2786	6773	12633

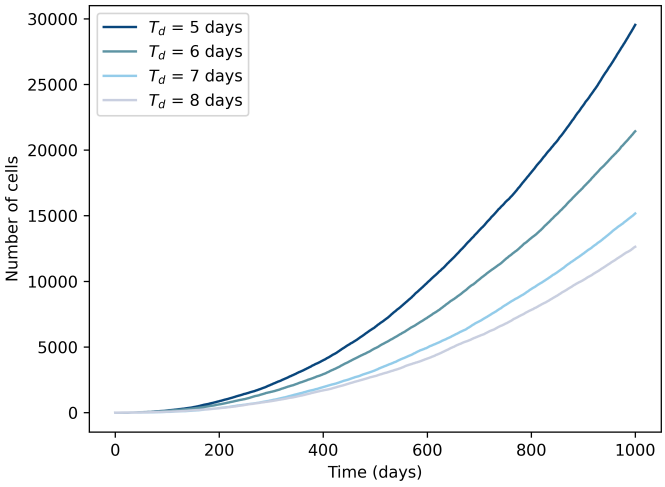

Figure 2: Uncontrolled proliferation model: tumor size $X(t)$ over 1000 days for mean division times $T_d = 5, 6, 7, 8$ days.

cellular automaton to a finite square domain of side length $2L+1$ centered at the origin:

$$\mathcal{D} = \{(i,j)\colon\ -L \le i,j \le L\}.$$

Division proceeds as in the unconstrained model, but a daughter cell can only be placed on a neighbor site if it lies within $\mathcal{D}$. Under these rules, cell proliferation saturates when most sites in $\mathcal{D}$ become occupied. The maximum tumor size is therefore

$$X_{\max} = \sum_{(i,j)\in\mathcal{D}} 1 = (2L+1)^2. \tag{4}$$

Simulation results exhibit an initial exponential growth phase followed by a plateau as $X(t)$ approaches $X_{\max}$. This sigmoidal behavior is consistent with classical Verhulst (logistic) dynamics and is widely used in mathematical oncology [11–17].

Simulation of spatially constrained tumor growth.

The CA model on the finite domain $\mathcal{D} = \{(i,j)\colon\ -L \le i,j \le L\}$ with $L = 50$ was simulated using $\Delta t = 1$ day and $T_d = 5$ days. The tumor size $X(t)$ was recorded and plotted in Fig. 3, demonstrating logistic-type saturation as

$X(t)$ approaches the plateau $X_{\max} = (2L+1)^2 = 10201$. The tumor sizes at selected time points for various mean division times are listed in Table 4.

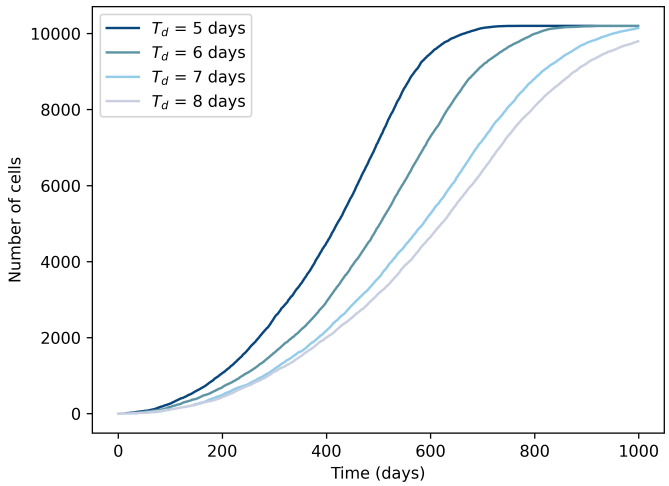

Figure 3: Spatially constrained proliferation model: growth curve $X(t)$ on the finite domain, showing sigmoidal saturation near $X_{\max} = 10201$.

Table 4: Tumor size $X(t)$ at $t = 250, 500, 750, 1000$ days for mean division times T_d under spatial constraint ($L = 50$).

T_d (days)	$t = 250$	$t = 500$	$t = 750$	$t = 1000$
5	1695	7176	10199	10201
6	1087	4929	9649	10201
7	780	3569	8083	10143
8	735	3157	7318	9798

3. Immune response model

In physiological conditions, tumor growth is restrained by the host immune system [5; 18–20]. Effector lymphocytes, specifically T cells, recognize and bind to abnormal cells such as cancer, forming a tumor-effector complex [21–23].

Let $x_{i,j}(t) \in \{0,1\}$ denote a tumor cell and $y_{i,j}(t) \in \{0,1\}$ an effector cell at site (i,j) and time t. Define the complex indicator

$$c_{i,j}(t) \;=\; x_{i,j}(t)\, y_{i,j}(t) \;\in \{0,1\}, \tag{5}$$

so that $c_{i,j}(t) = 1$ exactly when both a tumor cell and an effector occupy the same lattice site. Additionally, we denote the total effector cell population $Y(t) = \sum_{i,j} y_{i,j}(t)$ and the total tumor-effector complex population $C(t) = \sum_{i,j} c_{i,j}(t)$, in direct analogy to the tumor size $X(t)$.

The initial condition is

$$\begin{aligned} x_{0,0}(0) &= 1, \\ x_{i,j}(0) &= 0, \quad (i,j) \neq (0,0), \\ Y(0) &= 0, \quad C(0) = 0. \end{aligned} \tag{6}$$

i.e. one tumor cell at the origin and no effector cells or complexes.

Cell death.

Effector cells have mean lifetime T_y, giving per-step death probability

$$p_y = 1 - e^{-\frac{\Delta t}{T_y}}. \tag{7}$$

Tumor cells in complex die with mean lifetime T_x, yielding

$$p_x = 1 - e^{-\frac{\Delta t}{T_x}}. \tag{8}$$

When $c_{i,j}(t) = 1$, an effector may kill the tumor cell with probability p_x, and the effector itself may die of natural causes with probability p_y. Independent random draws determine whether each cell survives or is removed at that time step.

Tumor cell division.

Tumor cells not bound in a tumor-effector complex ($c_{i,j}(t) = 0$) divide using the same stochastic rule as in the uncontrolled proliferation model. At each time step, such a cell divides with probability p_d (1), placing its daughter on a randomly chosen empty von Neumann neighbor within the domain.

Regulatory effect of cytokines

Cytokines secreted by each tumor-effector complex diffuse rapidly through the tissue and decay exponentially with mean lifetime T_c. Under a quasi-steady approximation, the contribution of a single complex at lattice site (k, ℓ) to the cytokine level in cell (i, j) is

$$u_{i,j}^{(k,\ell)} = \alpha \int_0^\infty e^{-t/T_c} \frac{1}{4\pi D\, t}\, e^{-\frac{\Delta L^2((i-k)^2+(j-\ell)^2)}{4\,D\,t}}\, \mathrm{d}t, \tag{9}$$

where ΔL is the lattice spacing, α the secretion rate, D the diffusion coefficient, and t_C the cytokine lifetime [5]. The total cytokine concentration at (i, j) and time t is then

$$U_{i,j}(t) = \sum_{k,\ell} c_{k,\ell}(t)\; u_{i,j}^{(k,\ell)}.$$

Note that under the quasi-steady approximation, $u_{i,j}^{(k,\ell)}$ depends only on the spatial distance and not on time. Thus, one can precompute its values for all distances present in the lattice and store them in a lookup table. During simulation, these precomputed kernel values can be retrieved directly, significantly reducing computational overhead.

Effector cell movement.

Effector cells do not divide but migrate toward regions of high cytokine concentration, which correspond to active tumor-effector complexes. At each time step, an effector at lattice site (i, j) selects one of its four von Neumann neighbors

$$\mathcal{N}_{i,j} = \{(i+1, j), (i-1, j), (i, j+1), (i, j-1)\}$$

and moves into neighbor $(i', j') \in \mathcal{N}_{i,j}$ with probability

$$p_{i',j'} = \frac{1 + \chi\, U_{i',j'}(t)}{\sum_{(m,n)\in\mathcal{N}_{i,j}} \big(1 + \chi\, U_{m,n}(t)\big)},$$

where $U_{m,n}(t)$ is the cytokine concentration and χ is the chemotactic sensitivity [5]. This bias directs effector cells toward regions of active immune response.

If an effector moves into a site (i', j') already occupied by a tumor cell (i.e. $x_{i',j'}(t) = 1$), they immediately form a tumor-effector complex, setting $c_{i',j'}(t) = 1$.

Effector cells begin with zero population inside the domain (6) and enter exclusively through a one-cell-wide boundary ring. Let N_0 denote the constant

ambient effector concentration outside the lattice. Since the ring is exactly one lattice cell thick, its total entry length (excluding corner cells) is four sides of length $2L$. Hence the per-step influx probability is

$$p_{\text{in}} = 1 - e^{-8\,L\,N_0\,\Delta L}, \tag{10}$$

Upon an influx event, a new effector is placed at a uniformly random boundary site. Effector cells may also leave the domain by moving beyond its boundary.

Simulation of immune response model.

The model was simulated with the parameters listed in Table 5. Simulations were run from $t = 0$ until $t = 70$ days. To focus on immune-mediated clearance, effector influx was delayed until the tumor cell count reached 150-190 cells.

Under these conditions, in most trials the immune response eliminated the tumor between day 40 and day 70. Figure 4 shows the time courses of the tumor cell count, effector cell count, and tumor-effector complex count. Complexes vanish immediately upon tumor eradication, confirming the correctness of the implementation.

Table 5: Model parameters used in the simulations

Parameter	Value
Time step Δt	1 min
Tumor cell lifetime T_x	720 min (0.5 day)
Effector lifetime T_y	4320 min (3 days)
Cytokine lifetime T_c	720 min (0.5 day)
Tumor division time T_d	7200 min (5 days)
Cytokine rate α	1 cell/min
Ambient effector density N_0	4×10^{-6} cells/μm^2
Chemotactic sensitivity χ	1000
Boundary width ΔL	10 μm
Domain half-width L	500 μm
Diffusion coefficient D	2000 μm^2/min

Impact of chemotactic sensitivity.

To assess the role of cytokine-driven chemotaxis, we varied the sensitivity parameter χ while holding all other parameters fixed (Table 5). Figure 5

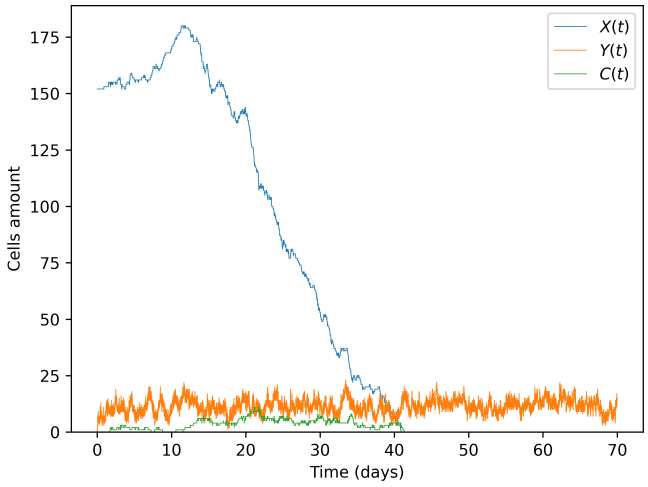

Figure 4: Time courses of tumor cells, effector cells, and tumor-effector complexes under the specified parameters are plotted over 70 days.

displays representative time courses of tumor cells, effector cells, and tumor-effector complexes for several different values of χ.

These results underscore the pivotal role of cytokine-mediated chemotaxis in orchestrating an effective antitumor response: sufficient chemotactic sensitivity enables rapid effector accumulation at tumor sites and decisive tumor control, whereas without chemotaxis effector cells wander aimlessly and fail to control tumor growth.

Impact of ambient effector density.

The ambient effector density N_0 governs the supply of new immune cells at the boundary. To assess its effect, we ran simulations for low and high values of N_0, holding all other parameters as in Table 5. Figure 6 shows representative time courses for these two scenarios.

These simulations underscore the critical role of immune influx: when effector supply is low, tumors grow unchecked, whereas a robust supply leads to rapid tumor clearance.

Impact of effector lifetime.

Effector lifetime T_y critically determines immune persistence in the tissue. To assess its effect, we compared short-lived and long-lived effectors while

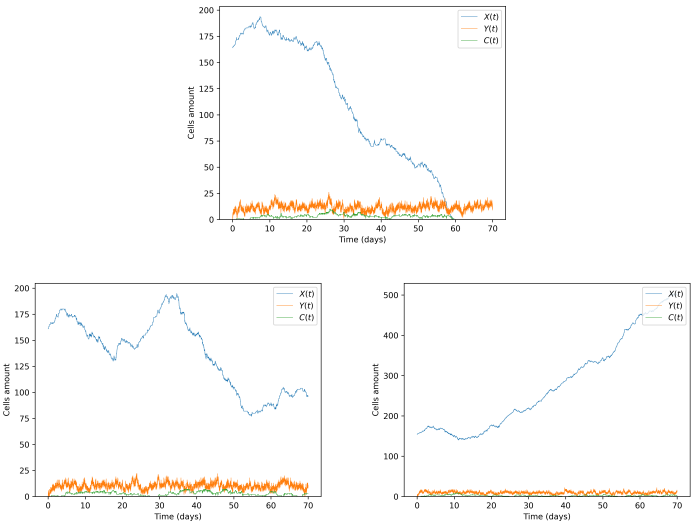

Figure 5: Simulation results under varying chemotactic sensitivity χ: $\chi = 1000$, $\chi = 500$, and $\chi = 0$, respectively. Tumor cells, effector cells, and tumor-effector complexes are plotted over 70 days.

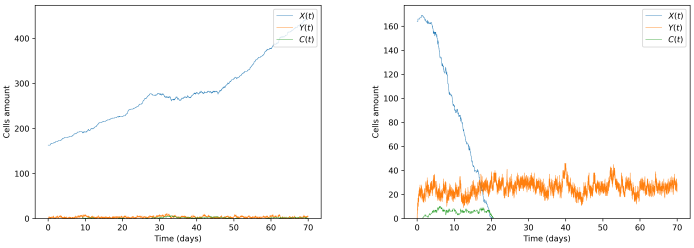

Figure 6: Simulation results under varying ambient effector density: (left) $N_0 = 10^{-6}$, (right) $N_0 = 10^{-5}$. Tumor cells, effector cells, and tumor-effector complexes are plotted over 70 days.

holding all other parameters fixed (Table 5). Figure 7 shows representative time courses for these two scenarios.

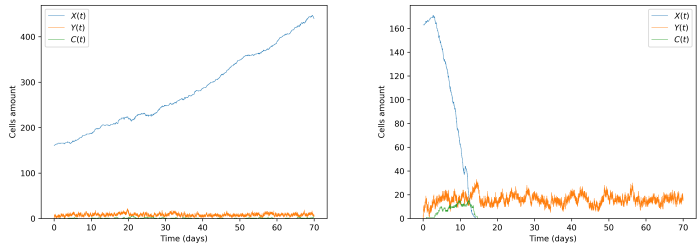

Figure 7: Simulation results under varying effector lifetime: (left) $T_y = 1$ day; (right) $T_y = 14$ days. Tumor cells, effector cells, and tumor-effector complexes over 70 days.

Short-lived effectors are removed too rapidly to establish sufficient tumor-effector interactions, allowing unchecked tumor expansion. In contrast, long-lived effectors persist in the tissue, accumulate at the tumor interface, and achieve complete tumor eradication. Thus, effector cell longevity is a key factor for sustained antitumor immunity in the model.

Conclusion

We demonstrated that cellular automata models of increasing complexity can both reproduce classical tumor growth laws and reveal key immune-tumor interactions. The uncontrolled-proliferation model yields exponential expansion, the spatially constrained model produces logistic-type saturation, and the immune response model shows how effector cell lifetime, chemotactic sensitivity, and boundary influx determine the balance between tumor eradication and escape.

Such a rule-based model is very flexible and can easily include different microenvironments, extra immune pathways, and therapeutic strategies. Moreover, as computational power increases, simulations will become increasingly efficient, making cellular automata models exceptionally promising as excellent aids for practical modeling of cancer and other complex biological processes.

References

1. Murray, J. D. (2002). *Mathematical biology I: An introduction* (3rd ed.). Springer.
2. Kansal, A. R., Torquato, E. C., Chiocca, S., & Deisboeck, T. S. (2000). Simulated brain tumour growth dynamics using a three-dimensional cellular automaton. *J. Theor. Biol., 203*, 367–382. https://doi.org/10.1006/jtbi.2000.2000
3. Verhulst, P. F. (1845). Recherches mathématiques sur la loi d'accroissement de la population. *Nouv. Mém. Acad. Roy. Sci. Belles-Lett. Brux., 18*, 1–41.
4. Kuznetsov, V. A., Makalkin, I. A., Taylor, M. A., & Perelson, A. S. (1994). Nonlinear dynamics of immunogenic tumors: Parameter estimation and global bifurcation analysis. *Bull. Math. Biol., 56*, 295–321. https://doi.org/10.1007/BF02460644
5. Cooper, A. K., & Kim, P. S. (2014). A cellular automata and a partial differential equation model of tumor-immune dynamics and chemotaxis. In *Mathematical models of tumor-immune system dynamics* (pp. 21–46). Springer. https://doi.org/10.1007/978-1-4939-1793-8_2
6. Laird, A. K. (1964). Dynamics of tumor growth. *Br. J. Cancer, 18*, 490–502. https://doi.org/10.1038/bjc.1964.55
7. Steel, G. G. (1977). *Growth kinetics of tumours: Cell population kinetics in relation to the growth and treatment of cancer*. Clarendon Press.
8. Benzekry, S., Lamont, C., Beheshti, A., Tracz, A., Ebos, J., Hlatky, L., & Hahnfeldt, P. (2014). Classical mathematical models for description and prediction of experimental tumor growth. *PLoS Comput. Biol., 10*, e1003800. https://doi.org/10.1371/journal.pcbi.1003800
9. Byrne, H. M., & Drasdo, D. (2009). Individual-based and continuum models of growing cell populations: A comparison. *J. Math. Biol., 58*, 657–687. https://doi.org/10.1007/s00285-008-0212-0
10. Anderson, A. R. A. (2005). A hybrid mathematical model of solid tumour invasion: The importance of cell adhesion. *IMA J. Math. Med. Biol., 22*, 163–186. https://doi.org/10.1093/imammb/dqi005
11. Tsoularis, A., & Wallace, J. (2002). Analysis of logistic growth models. *Math. Biosci., 179*, 21–55. https://doi.org/10.1016/S0025-5564(02)00096-2
12. Gerlee, P. (2013). The model muddle: In search of tumor growth laws. *Cancer Res., 73*, 2407–2411. https://doi.org/10.1158/0008-5472.CAN-12-4355
13. Tracqui, P. (2009). Biophysical models of tumour growth. *Rep. Prog. Phys., 72*, 056701. https://doi.org/10.1088/0034-4885/72/5/056701
14. Ward, J. P., & King, J. R. (1999). Mathematical modelling of avascular tumour growth II: Modelling growth saturation. *IMA J. Math. Med. Biol., 16*, 171–211. https://doi.org/10.1093/imammb/16.2.171
15. Enderling, H., & Chaplain, M. A. J. (2014). Mathematical modelling of tumour growth and treatment. *Curr. Pharm. Des., 20*, 4934–4940. https://doi.org/10.2174/1381612819666131125150434

16. Simeoni, M., Magni, P., Cammia, C., De Nicolao, G., Croci, V., Pesenti, E., Germani, M., Poggesi, I., & Rocchetti, M. (2004). Predictive pharmacokinetic–pharmacodynamic modeling of tumor growth kinetics in xenograft models after administration of anticancer agents. *Cancer Res., 64*, 1094–1101. https://doi.org/10.1158/0008-5472.can-03-2524

17. Norton, L. (1988). A Gompertzian model of human breast cancer growth. *Cancer Res., 48*, 7067–7071.

18. Dunn, G. P., Bruce, A. T., Ikeda, H., Old, L. J., & Schreiber, R. D. (2002). Cancer immunoediting: From immunosurveillance to tumor escape. *Nat. Immunol., 3*, 991–998. https://doi.org/10.1038/ni1102-991

19. Hanahan, D., & Weinberg, R. A. (2011). Hallmarks of cancer: The next generation. *Cell, 144*, 646–674. https://doi.org/10.1016/j.cell.2011.02.013

20. Schreiber, R. D., Old, L. J., & Smyth, M. J. (2011). Cancer immunoediting: Integrating immunity's roles in cancer suppression and promotion. *Science, 331*, 1565–1570. https://doi.org/10.1126/science.1203486

21. Kirschner, D., & Panetta, J. C. (1998). Modeling immunotherapy of the tumor–immune interaction. *J. Math. Biol., 37*, 235–252. https://doi.org/10.1007/s002850050127

22. de Pillis, L. G., Radunskaya, A. E., & Wiseman, C. L. (2005). A validated mathematical model of cell-mediated immune response to tumor growth. *Cancer Res., 65*, 7950–7958. https://doi.org/10.1158/0008-5472.CAN-05-0564

23. Eftimie, R., Bramson, J. L., & Earn, D. J. D. (2011). Interactions between the immune system and cancer: A brief review of non-spatial mathematical models. *Bull. Math. Biol., 73*, 2–32. https://doi.org/10.1007/s11538-010-9526-3

Рапчинський О., Кічмаренко О., Стехун А.

ДИСКРЕТНІ МОДЕЛІ КЛІТИННИХ АВТОМАТІВ ДИНАМІКИ РОСТУ ПУХЛИНИ ТА ІМУННОГО НАГЛЯДУ

Резюме

У статті досліджено дискретні моделі клітинних автоматів для опису динаміки росту пухлини та імунного нагляду. Розглянуто три моделі зростаючої складності: модель неконтрольованої проліферації, яка відтворює експоненціальне розширення пухлинної популяції; модель проліферації з просторовими обмеженнями, що демонструє логістичне насичення, зумовлене обмеженістю мікрооточення; а також модель імунної відповіді, яка враховує взаємодію ефекторних клітин із пухлинними клітинами та хемотаксис, опосередкований цитокінами. Моделі реалізовано на двовимірних ґратках із використанням стохастичних правил оновлення, параметризованих біологічно обґрунтованими швидкостями поділу та загибелі клітин. Чисельні експерименти показують, що модель неконтрольованого росту відтворює класичну експоненціальну динаміку, тоді як модель із просторовими обмеженнями приводить до S-подібних кривих росту, узгоджених із динамікою Ферхюльста. Модель імунної відповіді дозволяє моделювати взаємодію пухлинних клітин, ефекторних лімфоцитів і цитокінових сигналів, виявляючи складні біологічні режими, які важко описати суто аналітичними методами. Аналіз чутливості параметрів виявляє критичні режими секреції цитокінів та рекрутування ефекторних клітин, що визначають перехід між стримуванням пухлини та її імунним уникненням.
Ключові слова: клітинні автомати, ріст пухлини, моделювання, імунна відповідь, хемотаксис.

Список літератури

1. Murray, J. D. (2002). *Mathematical biology I: An introduction* (3rd ed.). Springer.
2. Kansal, A. R., Torquato, E. C., Chiocca, S., & Deisboeck, T. S. (2000). Simulated brain tumour growth dynamics using a three-dimensional cellular automaton. *J. Theor. Biol., 203*, 367–382. https://doi.org/10.1006/jtbi.2000.2000
3. Verhulst, P. F. (1845). Recherches mathématiques sur la loi d'accroissement de la population. *Nouv. Mém. Acad. Roy. Sci. Belles-Lett. Brux., 18*, 1–41.
4. Kuznetsov, V. A., Makalkin, I. A., Taylor, M. A., & Perelson, A. S. (1994). Nonlinear dynamics of immunogenic tumors: Parameter estimation and global bifurcation analysis. *Bull. Math. Biol., 56*, 295–321. https://doi.org/10.1007/BF02460644
5. Cooper, A. K., & Kim, P. S. (2014). A cellular automata and a partial differential equation model of tumor-immune dynamics and chemotaxis. In *Mathematical models of tumor-immune system dynamics* (pp. 21–46). Springer. https://doi.org/10.1007/978-1-4939-1793-8_2
6. Laird, A. K. (1964). Dynamics of tumor growth. *Br. J. Cancer, 18*, 490–502. https://doi.org/10.1038/bjc.1964.55

7. Steel, G. G. (1977). *Growth kinetics of tumours: Cell population kinetics in relation to the growth and treatment of cancer*. Clarendon Press.

8. Benzekry, S., Lamont, C., Beheshti, A., Tracz, A., Ebos, J., Hlatky, L., & Hahnfeldt, P. (2014). Classical mathematical models for description and prediction of experimental tumor growth. *PLoS Comput. Biol., 10*, e1003800. https://doi.org/10.1371/journal.pcbi.1003800

9. Byrne, H. M., & Drasdo, D. (2009). Individual-based and continuum models of growing cell populations: A comparison. *J. Math. Biol., 58*, 657–687. https://doi.org/10.1007/s00285-008-0212-0

10. Anderson, A. R. A. (2005). A hybrid mathematical model of solid tumour invasion: The importance of cell adhesion. *IMA J. Math. Med. Biol., 22*, 163–186. https://doi.org/10.1093/imammb/dqi005

11. Tsoularis, A., & Wallace, J. (2002). Analysis of logistic growth models. *Math. Biosci., 179*, 21–55. https://doi.org/10.1016/S0025-5564(02)00096-2

12. Gerlee, P. (2013). The model muddle: In search of tumor growth laws. *Cancer Res., 73*, 2407–2411. https://doi.org/10.1158/0008-5472.CAN-12-4355

13. Tracqui, P. (2009). Biophysical models of tumour growth. *Rep. Prog. Phys., 72*, 056701. https://doi.org/10.1088/0034-4885/72/5/056701

14. Ward, J. P., & King, J. R. (1999). Mathematical modelling of avascular tumour growth II: Modelling growth saturation. *IMA J. Math. Med. Biol., 16*, 171–211. https://doi.org/10.1093/imammb/16.2.171

15. Enderling, H., & Chaplain, M. A. J. (2014). Mathematical modelling of tumour growth and treatment. *Curr. Pharm. Des., 20*, 4934–4940. https://doi.org/10.2174/1381612819666131125150434

16. Simeoni, M., Magni, P., Cammia, C., De Nicolao, G., Croci, V., Pesenti, E., Germani, M., Poggesi, I., & Rocchetti, M. (2004). Predictive pharmacokinetic–pharmacodynamic modeling of tumor growth kinetics in xenograft models after administration of anticancer agents. *Cancer Res., 64*, 1094–1101. https://doi.org/10.1158/0008-5472.can-03-2524

17. Norton, L. (1988). A Gompertzian model of human breast cancer growth. *Cancer Res., 48*, 7067–7071.

18. Dunn, G. P., Bruce, A. T., Ikeda, H., Old, L. J., & Schreiber, R. D. (2002). Cancer immunoediting: From immunosurveillance to tumor escape. *Nat. Immunol., 3*, 991–998. https://doi.org/10.1038/ni1102-991

19. Hanahan, D., & Weinberg, R. A. (2011). Hallmarks of cancer: The next generation. *Cell, 144*, 646–674. https://doi.org/10.1016/j.cell.2011.02.013

20. Schreiber, R. D., Old, L. J., & Smyth, M. J. (2011). Cancer immunoediting: Integrating immunity's roles in cancer suppression and promotion. *Science, 331*, 1565–1570. https://doi.org/10.1126/science.1203486

21. Kirschner, D., & Panetta, J. C. (1998). Modeling immunotherapy of the tumor–immune interaction. *J. Math. Biol., 37*, 235–252. https://doi.org/10.1007/s002850050127

22. de Pillis, L. G., Radunskaya, A. E., & Wiseman, C. L. (2005). A validated mathematical model of cell-mediated immune response to tumor growth. *Cancer Res., 65*, 7950–7958. https://doi.org/10.1158/0008-5472.CAN-05-0564

23. Eftimie, R., Bramson, J. L., & Earn, D. J. D. (2011). Interactions between the immune system and cancer: A brief review of non-spatial mathematical models. *Bull. Math. Biol., 73*, 2–32. https://doi.org/10.1007/s11538-010-9526-3